



Article

Conformational Equilibrium of NADPH–Cytochrome P450 Oxidoreductase Is Essential for Heme Oxygenase Reaction

Masakazu Sugishima ^{1,*} , Junichi Taira ², Tatsuya Sagara ², Ryota Nakao ², Hideaki Sato ¹ , Masato Noguchi ¹, Keiichi Fukuyama ³, Ken Yamamoto ¹, Takuo Yasunaga ² and Hiroshi Sakamoto ^{2,*}

¹ Department of Medical Biochemistry, Kurume University School of Medicine, 67 Asahi-machi, Kurume 830-0011, Japan; hsato@med.kurume-u.ac.jp (H.S.); miwata2410@384.jp (M.N.); yamamoto_ken@med.kurume-u.ac.jp (K.Y.)

² Department of Bioscience and Bioinformatics, Graduate School of Computer Science and Systems Engineering, Kyushu Institute of Technology, 680-4 Kawazu, Iizuka 820-8502, Japan; taira@bio.kyutech.ac.jp (J.T.); supersonic.runrun@gmail.com (T.S.); nakryo@gmail.com (R.N.); yasunaga@bio.kyutech.ac.jp (T.Y.)

³ Department of Biological Sciences, Graduate School of Science, Osaka University, 1-1 Machikaneyama-cho, Toyonaka 560-0043, Japan; fukuyamakei1@gmail.com

* Correspondence: sugishima_masakazu@med.kurume-u.ac.jp (M.S.); sakakan@bio.kyutech.ac.jp (H.S.)

Received: 11 June 2020; Accepted: 22 July 2020; Published: 28 July 2020



Abstract: Heme oxygenase (HO) catalyzes heme degradation using electrons supplied by NADPH–cytochrome P450 oxidoreductase (CPR). Electrons from NADPH flow first to FAD, then to FMN, and finally to the heme in the redox partner. Previous biophysical analyses suggest the presence of a dynamic equilibrium between the open and the closed forms of CPR. We previously demonstrated that the open-form stabilized CPR (Δ TGEE) is tightly bound to heme–HO-1, whereas the reduction in heme–HO-1 coupled with Δ TGEE is considerably slow because the distance between FAD and FMN in Δ TGEE is inappropriate for electron transfer from FAD to FMN. Here, we characterized the enzymatic activity and the reduction kinetics of HO-1 using the closed-form stabilized CPR (147CC514). Additionally, we analyzed the interaction between 147CC514 and heme–HO-1 by analytical ultracentrifugation. The results indicate that the interaction between 147CC514 and heme–HO-1 is considerably weak, and the enzymatic activity of 147CC514 is markedly weaker than that of CPR. Further, using cryo-electron microscopy, we confirmed that the crystal structure of Δ TGEE in complex with heme–HO-1 is similar to the relatively low-resolution structure of CPR complexed with heme–HO-1 in solution. We conclude that the “open–close” transition of CPR is indispensable for electron transfer from CPR to heme–HO-1.

Keywords: analytical ultracentrifuge; cryo-electron microscopy; electron transfer; protein–protein interaction

1. Introduction

Heme oxygenase (HO, EC 1.14.14.18) catalyzes the degradation of heme to biliverdin, CO, and ferrous ion [1–3] by utilizing reducing equivalents derived from NADPH–cytochrome P450 reductase (CPR, EC 1.6.2.4). The major physiological roles of an inducible isoform of HO, HO-1, in mammals are the maintenance of iron homeostasis by the recycling of iron and the defense against oxidative stress by the detoxification of heme, a pro-oxidant, and the production of bilirubin, a potent antioxidant. CO, produced by HO-1 and a constitutive isoform, HO-2, mediates various types of

cell activities, such as anti-inflammatory, anti-apoptotic, and vasodilatory activities [4,5]. The HO reaction proceeds via three reaction intermediates: α -hydroxyheme, α -verdoheme, and biliverdin-iron chelate. CO is produced in the conversion from α -hydroxyheme to α -verdoheme. At least three of four reaction steps, reducing equivalents supplied by CPR, are required. In total, seven electrons are required for a cycle of reaction to produce biliverdin and ferrous ion from heme. Biliverdin is subsequently converted to bilirubin by biliverdin reductase [6–8]. Almost all crystal structures of HO complexed with its substrates, reaction intermediates, and product have been determined [9–19].

CPR is a member of a family of diflavin reductases, which catalyzes electron transfer from NADPH to FAD, FMN, and finally the heme groups in their redox partners [20,21]. Rat CPR (rCPR) is composed of three domains: the FMN-binding domain (residues 77–232), the ferredoxin-NADP⁺ oxidoreductase (FNR)-like domain (residues 267–325 and 450–678), and the connecting domain (residues 244–266 and 326–450). The connecting domain and the FNR-like domain jointly form the FAD-binding domain, wherein the NADPH-binding site is present. The FAD and FMN-binding domains are connected by a flexible hinge formed by a span of 12 residues, from Gly232 to Arg243, in rCPR.

For electron transfer to occur, CPR and its redox partners must associate with one another. The first reported CPR structure was observed to have a closed conformation, in which NADP⁺, FAD, and FMN were in close proximity, which was suitable for intramolecular electron transfer [22]. However, it is hardly probable that redox partners such as cytochrome P450 could be positioned close enough to FMN for intermolecular electron transfer to occur.

Hamdane et al. developed an rCPR mutant in which four consecutive residues in the hinge region (from Thr236 to Glu239) were removed (hereafter referred to as Δ TGEE). They determined the crystal structure of Δ TGEE and observed three remarkably extended conformations (open conformation). In the open conformation, the distance between FAD and FMN coenzymes were in the range of 30–60 Å [23]. The structures of Δ TGEE indicate that the FMN-binding domain is highly mobile compared to the rest of the molecule, whereby the open conformation of CPR is able to bind its redox partner. Recently, we were able to determine the crystal structure of Δ TGEE complexed with heme-rat HO-1 (rHO-1) [24] and observed that Δ TGEE could bind its redox partner tightly and change its conformation marginally upon NADP⁺/NADPH binding [25]. The results of the NMR analysis of HO-2 complexed with CPR [26] are consistent with the crystallographic results. However, the distance between FAD and FMN in the complex is considerably large to allow direct electron transfer, and the reduction kinetics of heme-HO-1 in the presence of the NADPH- Δ TGEE system is 360-fold slower than that in the presence of the NADPH-rCPR system. Moreover, Xia et al. developed an rCPR mutant in which the salt bridge (Asp147-Arg514) between the FMN-binding and the FAD-binding domains in the closed conformation was replaced by a disulfide bridge to stabilize the closed conformation (hereafter referred to as 147CC514) [27]. Intramolecular electron transfer in 147CC514 was impaired by the rotation of FMN by 20° and the weakened affinity of NADPH, while the rate of hydride transfer from NADPH to FAD was moderately reduced. Intermolecular electron transfer to cytochrome *c* and cytochrome P450 was severely impaired by 147CC514. Further, it was reported that these transfers were restored upon cleavage of the disulfide bond in 147CC514 in response to the addition of dithiothreitol (DTT). These data suggest that the “open-close” transition of CPR is necessary for a smooth electron transfer. Computational simulation provided evidence of the “open-close” transition of CPR with the redox change in its coenzymes [28].

However, to complete a catalytic cycle, HO utilizes seven electrons supplied by CPR, whereas cytochrome P450 utilizes only two electrons. Since electron transfer from CPR to heme-HO-1 occurs sequentially, seven cycles of “open-close” transition of CPR are required for a single cycle of HO reaction. During the HO reaction, oxygen-labile reaction intermediates such as α -hydroxyheme and α -verdoheme are formed. Therefore, if the electron transfer cycle from CPR to HO is considerably slow, these intermediates may be decomposed before they can accept the next electron. However, such decomposition does not occur under physiological conditions. To validate the current electron transfer model, we characterized the HO reaction and the reduction kinetics of heme-rHO-1 in the

presence of the NADPH–147CC514 system. Further, we characterized the interaction of heme–rHO-1 with rCPR, Δ TGEE, and 147CC514 by analytical ultracentrifugation. In addition, we confirmed that the structure of rCPR complexed with heme–rHO-1 in solution is similar to the crystal structure of the Δ TGEE–heme–HO-1 complex, using single-particle analysis in cryo-electron microscopy in spite of its low resolution. On the basis of these results, we confirmed that the “open–close” transition of CPR is necessary for a smooth electron transfer from CPR to heme–HO-1.

2. Materials and Methods

2.1. Protein Expression and Purification

Both rCPR and rHO-1 are membrane-bound proteins anchored to the cytoplasmic surface of the endoplasmic reticulum. To handle these conveniently, we prepared soluble forms of rHO-1, rCPR, Δ TGEE, and 147CC514 by removing their membrane-spanning regions. rHO-1, rCPR, and Δ TGEE were expressed in *Escherichia coli* and purified as described earlier [23,24,29,30]. An expression vector was constructed for 147CC514 using the synthesized cDNA (FASMAC, Atsugi, Japan) of rCPR in which Asp147 and Arg514 were substituted with cysteine residues, and except for the catalytic cysteine (Cys630), the other cysteine residues in rCPR not containing the membrane-spanning region (Met1–Ile57), were substituted with amino acid residues to form Cys136Ala, Cys228Ala, Cys363Thr, Cys445Leu, and Cys472Thr [27]. The resultant cDNA of 147CC514 was subcloned into a pET-21a(+) expression vector (Merck, Darmstadt, Germany) for the expression of the non-His tagged enzyme, using an in-fusion HD cloning kit (Takara Bio, Kusatsu, Japan) and the appropriate primers. The pET-21a-147CC514 plasmid formed, in which the open reading frame (ORF) sequence was confirmed by DNA sequencing, was transformed into RosettaGami B (DE3) (Merck), followed by overnight culturing of the transformed *E. coli* at 37 °C on Luria–Bertani (LB)–agar plates containing 100 μ g/mL ampicillin and 33 μ g/mL chloramphenicol. A single colony was selected to inoculate 3 mL of LB medium containing 100 μ g/mL ampicillin and 33 μ g/mL chloramphenicol; 1.6 mL of the overnight culture was used to inoculate 400 mL of LB medium containing 100 μ g/mL ampicillin, 33 μ g/mL chloramphenicol, and 10 μ g/mL riboflavin. The cells were cultured in baffled flasks at 37 °C with shaking at 240 rpm for 3 h, at which point isopropyl β -D-1-thiogalactopyranoside (IPTG) was added to a final concentration of 100 μ M to initiate reductase expression. The cultures were incubated for an additional 72 h at 19 °C with shaking at 130 rpm.

The cells expressing 147CC514 were sonicated in a solution with 50 mM Tris/HCl (pH 8.0), 2 mM EDTA (pH 8.0), 20% (v/v) glycerol, and 0.1% (v/v) Triton X-100. The mixture was incubated on ice for 3 h. Next, the insoluble fraction was removed by centrifugation. The 147CC514 protein was purified by the method used for rCPR purification [30], using anion-exchange, affinity, and hydroxyapatite columns with slight modifications (addition of 0.1% Triton X-100). Briefly, the supernatant was loaded in a Hitrap Q HP column (GE Healthcare, Chicago, IL, USA) equilibrated with 20 mM Tris/HCl (pH 7.4), 0.1 mM EDTA, 20% glycerol, and 0.1% Triton X-100. The yellow fractions eluted with a linear gradient of potassium chloride were collected. Subsequently, the collected fractions were introduced into a 2',5'-ADP Sepharose column (GE Healthcare) equilibrated with 5 mM potassium phosphate (pH 7.7), 20% glycerol, and 0.1% Triton X-100. After washing with the equilibration buffer and adding 0.7 mM NAD⁺, the 147CC514 fraction was eluted using the equilibration buffer, adding 0.7 mM NADP⁺. Excess NADP⁺ was removed using a Bio-Scale Mini CHT Type I Cartridge (Bio-Rad, Hercules, CA, USA) equilibrated with 5 mM potassium phosphate (pH 7.7) and 20% glycerol. The formation of the disulfide bond between Cys147 and Cys514 was confirmed by X-ray crystallography (Figure S1A, Table S1). The crystallization conditions were the same as reported by Xia et al. [27]. Diffraction data were merged and scaled with XDS package [31]. The model (PDB ID: 3OJW) was refined with Refmac5 [32] in CCP4 package [33]. The overall structure appeared to be almost identical to that reported by Xia et al. [27], although some loops (239–241, 501–504, and 598–600) were disordered in our refined model (Figure S1B). NADP⁺ was bound to the crystal, whereas the electron density of the

adenine ring of NADP⁺ was low. The electron density of the nicotinamide ring of NADP⁺ and that of rCPR were low as well [22].

DTT-treated and 2-iodoacetamide (IAM)/DTT-treated 147CC514 were prepared according to the method reported by Xia et al. [27]. Briefly, DTT-treated 147CC514 was prepared by incubating 147CC514 with DTT for 40 h at 4 °C in the UNILab Pro Glove Box (MBRAUN, Garching bei München, Germany), following which, the excess DTT was removed using a Zeba desalt spin column (Thermo Fisher Scientific, Waltham, MA, USA). Subsequently, IAM/DTT-treated 147CC514 was prepared by incubation of the DTT-treated 147CC514 with IAM for 30 min at 25 °C in an anaerobic chamber, following which, excess IAM was removed using a Zeba desalt spin column. To completely remove DTT or IAM, the samples were desalted twice in each step. For the control experiments, DTT-treated rCPR and IAM/DTT-treated rCPR were prepared according to the method used for 147CC514 preparation. The concentrations of rCPR, ΔTGEE, and 147CC514 were determined by measuring the absorbance at 454 nm with a molar extinction coefficient (ϵ) of 21.4 mM⁻¹ cm⁻¹.

The heme-rHO-1 complex was reconstituted with 1.2 equiv. of heme and purified by column chromatography on a hydroxyapatite column (Bio-Rad), as previously described [34]. The concentration of heme-rHO-1 was determined by measuring the absorbance at 406 nm ($\epsilon = 140$ mM⁻¹ cm⁻¹) (pH 7.4). Rat biliverdin reductase used for the enzymatic assay was expressed in *E. coli* and purified by ammonium sulfate fractionation, affinity chromatography (2',5'-ADP Sepharose), and size-exclusion chromatography (Sephacryl S-200 HR (GE Healthcare)) [7,35].

2.2. Enzymatic Assay

HO activity in the NADPH-CPR system was determined based on the rate of bilirubin formation, which was monitored by the increase in the absorbance at 468 nm at 37 °C [36]. Bilirubin formation from biliverdin was catalyzed by biliverdin reductase present in the assay mixture, which contained 40 μM heme, 0.5 μM rHO-1, 0.5–2 μM rCPR—or 4–12 μM 147CC514, 1–1.5 μM IAM/DTT-treated rCPR, or 1–2 μM IAM/DTT-treated 147CC514—0.5 mg/mL bovine serum albumin, 12.5 μg/mL catalase, 6.7 μg/mL biliverdin reductase, and 250 μM NADPH in 0.1 M potassium phosphate buffer (pH 7.4). The assay commenced upon the addition of NADPH. A typical example of the assay is shown in Figure S2A.

Single turnover reactions were monitored based on changes in the absorption spectra at 30 °C. The reaction mixtures (0.1 mL) consisted of 4.3 μM heme-rHO-1, 40 nM rCPR or 100 nM 147CC514, and 25 μM NADPH in 0.1 M potassium phosphate buffer (pH 7.4). The spectra were recorded over a range of 300–900 nm.

Heme reduction was monitored based on changes in the absorption spectra at 30 °C in a CO-saturated anaerobic atmosphere. The CO-saturated reaction mixtures (0.1 mL) consisted of 4.3 μM heme-rHO-1, 10–30 nM rCPR—or DTT-treated 147CC514 or 10–100 nM 147CC514—and 25 μM NADPH in 0.1 M potassium phosphate buffer (pH 7.4). The reaction commenced upon the addition of NADPH. The initial rates of reduction of ferric heme-rHO-1 were calculated based on the decrease in the absorbance at 406 nm and the increase in the absorbance at 420 nm. The differences in ϵ between the ferric heme-rHO-1 and CO-bound ferrous heme-rHO-1 were 82.2 mM⁻¹ cm⁻¹ at 406 nm and 131 mM⁻¹ cm⁻¹ at 420 nm. A typical example is shown in Figure S2B. The mean values of the initial rates obtained were plotted against the concentration of rCPR. The rate constants for the reduction of heme in heme-rHO-1 were determined from the slope of the fitted line. The concentration of NADPH used in all assays was determined by measuring the absorbance at 340 nm ($\epsilon = 6.22$ mM⁻¹ cm⁻¹). A Cary 50 Bio UV-visible spectrophotometer (Varian, Palo Alto, CA, USA) was used for spectroscopic measurements in the enzymatic assay.

2.3. Analytical Ultracentrifugation

Sedimentation equilibrium experiments were performed at 25 °C in 0.1 M potassium phosphate buffer (pH 7.4) in an Optima XL-A analytical ultracentrifuge (Beckman Coulter, Brea, CA, USA)

with an An-60 Ti rotor. The data were acquired using the ProteomeLab XL-A software (Beckman Coulter). The mixtures of heme-rHO-1 and the equimolar CPR samples—rCPR, ΔTGEE, 147CC514, or IAM/DTT-treated 147CC514—were subjected to sedimentation equilibrium analysis. Aliquots of the protein solutions (120 μL) and reference buffer (140 μL) were loaded into a sedimentation equilibrium cell equipped with a double-sector charcoal-Epon centerpiece (12 mm path length). Following a 24 h equilibration period at 15,000 rpm, the absorbance was measured as a function of the radial position. The absorbance at 455 nm was measured in step mode with a step size of 0.001 cm and 18 replicates at each radial position. The solvent density (ρ) and partial specific volume (\bar{v}) were calculated using the SEDNTERP software (<http://www.rasmb.bbri.org>), and data analysis was performed using the Origin 9 software (OriginLab, Northampton, MA, USA). The sedimentation equilibrium data were fitted to a complex model, representing HO-1 + CPR \rightleftharpoons HO-1•CPR equilibrium (Equation (1)) [37].

$$A(r) = A_{\text{HO-1}}(r_0) \exp \{ M_{\text{HO-1}} H_{\text{HO-1}} (r^2 - r_0^2) \} + A_{\text{CPR}}(r_0) \exp \{ M_{\text{CPR}} H_{\text{CPR}} (r^2 - r_0^2) \} + K_{\text{HO-1}\cdot\text{CPR}} A_{\text{HO-1}}(r_0) A_{\text{CPR}}(r_0) \exp \{ (M_{\text{HO-1}} H_{\text{HO-1}} + M_{\text{CPR}} H_{\text{CPR}})(r^2 - r_0^2) \} + \delta \quad (1)$$

The data were also fitted to a non-complexed model in which two proteins exist in a monomeric state (Equation (2)).

$$A(r) = A_{\text{HO-1}}(r_0) \exp \{ M_{\text{HO-1}} H_{\text{HO-1}} (r^2 - r_0^2) \} + A_{\text{CPR}}(r_0) \exp \{ M_{\text{CPR}} H_{\text{CPR}} (r^2 - r_0^2) \} + \delta \quad (2)$$

In these equations, $A(r)$ represents the total sample absorbance as a function of the radial position, r ; $A_{\text{HO-1}}(r_0)$ and $A_{\text{CPR}}(r_0)$ represent the absorbances of monomeric heme-rHO-1 and CPRs at a reference position (r_0), respectively; $M_{\text{HO-1}}$ and M_{CPR} represent the average values of the molecular weights of heme-rHO-1 and CPRs, respectively; δ represents a minor baseline error correction term; $H = (1 - \bar{v}\rho)\omega^2/2RT$, where ω represents the angular velocity of the rotor, R represents the gas constant, and T represents the absolute temperature; $K_{\text{HO-1}\cdot\text{CPR}}$ represents the association constant on the absorbance concentration scale, $K_{\text{HO-1}\cdot\text{CPR}} = A_{\text{HO-1}\cdot\text{CPR}}/A_{\text{HO-1}} A_{\text{CPR}}$. To determine the dissociation constant (K_d), $K_{\text{HO-1}\cdot\text{CPR}}$ was converted to the molar scale as follows:

$$K_d = \left(\frac{\epsilon_{\text{HO-1}} + \epsilon_{\text{CPR}}}{\epsilon_{\text{HO-1}} \epsilon_{\text{CPR}} l} \right) \left(\frac{1}{K_{\text{HO-1}\cdot\text{CPR}}} \right) \quad (3)$$

where $\epsilon_{\text{HO-1}}$ and ϵ_{CPR} represent the molar extinction coefficients of heme-HO-1 and CPRs, respectively, and l represents the optical path length. The ϵ ($\text{mM}^{-1} \text{cm}^{-1}$) values of heme-rHO-1, rCPR, ΔTGEE, 147CC514, and IAM/DTT-treated 147CC514 at 455 nm were 15.1, 24.0, 23.8, 23.7, and 23.8, respectively.

2.4. Cryo-Electron Microscopy (EM), Image Processing, and Molecular Modeling of the rCPR-Heme-rHO-1 Complex

Specimens of the rCPR-heme-rHO-1 complex were quick-frozen using liquid ethane and stored in liquid nitrogen. In brief, 5 μL of the heme-rHO-1 (2 μM, 0.06 mg/mL) and rCPR (1.4 μM, 0.10 mg/mL) mixture in 0.1 M potassium phosphate buffer (pH 7.4) containing 2 μM NADP⁺ was mounted on a holey carbon grid and blotted with filter paper to remove the excess liquid and create a thin aqueous layer. The grid was then plunged into an ethane slash at −185 °C to create a thin layer of vitreous ice. The prepared specimens were examined at normal liquid nitrogen temperature using a CT3500 cryo-holder (Oxford Instruments, Abingdon-on-Thames, UK) and was further subjected to EM. Cryo-electron micrographs were captured using an electron microscope (EF-2000, Hitachi, Tokyo, Japan) equipped with an Si2048-CFX (DALSA-MedOptics, Tucson, AZ, USA) CCD camera [38]. The EM conditions were as follows: acceleration voltage, 200 kV; defocusing values, 1 to 3 μm for contrast enhancement; direct magnification, 140 k. After contrast transfer function compensation, 513 particles (128 × 128 pixel/image) were interactively selected from the micrographs (Figure S3). Three-dimensional molecular modeling was performed using an extensible object-oriented system

(Eos), as reported previously [39,40]. The overall resolution obtained for the reconstructed map of rCPR-heme-HO-1 was calculated as 25 Å by FSC_{0.5}.

3. Results

3.1. Enzymatic Assay

First, we determined the enzymatic activities of rHO-1 in the NADPH-147CC514 system. The rate of bilirubin formation was $1.96 \pm 0.35 \text{ min}^{-1}$ (N = 3) in the NADPH-rCPR system, compared to $0.229 \pm 0.0037 \text{ min}^{-1}$ (N = 4) in the NADPH-147CC514 system (Figure 1, Table 1). Therefore, the activity was 8.6-fold lower in the 147CC514 system. This is consistent with previous assays that used cytochrome P450 2B4; cytochrome P450 activity in the NADPH-membrane-bound 147CC514 system was 9.3-fold lower than that in the NADPH-membrane-bound CPR system [27]. We also assessed rHO-1 activity in the presence of IAM/DTT-treated 147CC514, in which the disulfide bond between Cys147 and Cys514 was cleaved, and both cysteine residues were alkylated to prevent re-formation of the disulfide bond during the enzymatic assay. rHO-1 activity was similar in the NADPH-IAM/DTT-treated 147CC514 system and the NADPH-IAM/DTT-treated rCPR system, although the values were almost 60% of that obtained in the presence of non-treated rCPR ($1.17 \pm 0.0024 \text{ min}^{-1}$ for IAM/DTT-treated rCPR and $1.25 \pm 0.197 \text{ min}^{-1}$ for IAM/DTT-treated 147CC514).

Table 1. Summary of the enzymatic assays. HO, heme oxygenase; rCPR, rat cytochrome P450 reductase; DTT, dithiothreitol; IAM, 2-iodoacetamide.

Reduction System	HO Activity		Apparent Reduction Rate Constant	
	(min ⁻¹)	(%)	(min ⁻¹)	(%)
rCPR	1.96 ± 0.35	100	122 ± 3.8	100
147CC514	0.229 ± 0.0037	11.7 ± 0.19	23.9 ± 5.1	19.6 ± 4.2
DTT-treated rCPR	ND	ND	130 ± 10.8	107 ± 8.9
DTT-treated 147CC514	ND	ND	112 ± 23.6	91.8 ± 19
IAM/DTT-treated rCPR	1.17 ± 0.0024	59.7 ± 0.12	ND	ND
IAM/DTT-treated 147CC514	1.25 ± 0.197	63.8 ± 10	ND	ND
ΔTGEE [24]	ND	ND	0.250	0.205

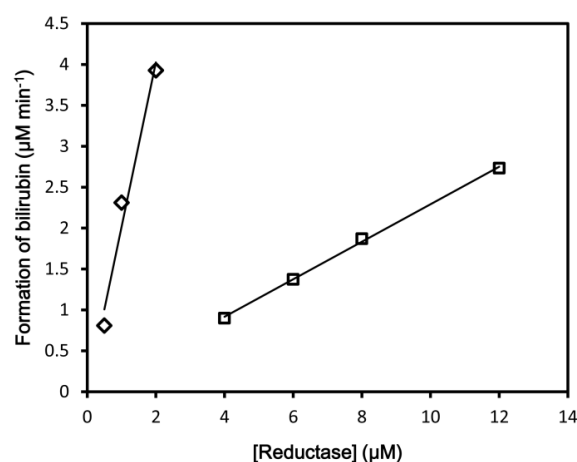


Figure 1. HO-1 activity. Bilirubin formation rates obtained in the NADPH-rCPR and NADPH-147CC514 systems were plotted as blank diamonds and squares, respectively. A representative example of the multiple measurements performed is displayed. See Methods for details.

As stated above, the HO reaction is fairly complex and requires seven electrons from CPR. It is interesting to examine the action of 147CC514 in the HO reaction system. Therefore, we observed the single turnover HO reaction in the NADPH-147CC514 system. In the NADPH-rCPR (0.04 μM) system,

the oxy-form was formed immediately, following which, the CO-verdoheme and the verdoheme forms appeared. Within 30 min, the heme residue was completely converted to biliverdin (Figure 2A). This appears to be similar to the reaction occurring in the NADPH–147CC514 (0.1 μM) system (Figure 2B).

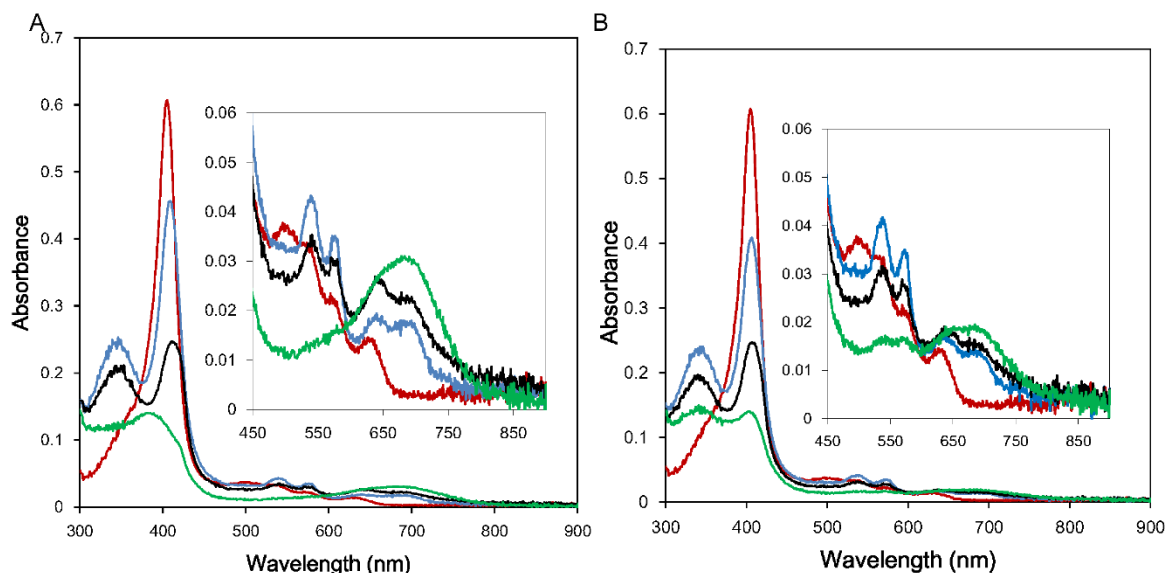


Figure 2. Changes in the absorption spectra of 4.3 μM heme-rHO-1 during the single turnover reaction in the presence of NADPH-rCPR or NADPH-147CC514. (A) Reaction with 0.04 μM rCPR. The spectra were recorded before (red) and 30 sec (cyan), 3.5 min (black), and 30 min (green) after NADPH addition. (B) Reaction with 0.1 μM 147CC514. The spectra were recorded before (red) and 3 min (cyan), 10 min (black), and 40 min (green) after NADPH addition. Magnified views of the visible region are shown in the insets.

3.2. Reduction Kinetics

The reduction rate of the ferric heme iron in heme-rHO-1 was measured by the rate of formation of CO-bound heme-rHO-1 in a CO-saturated atmosphere. The apparent reduction rate constants for the heme reduction of heme-rHO-1 were determined to be $122 \pm 3.8 \text{ min}^{-1}$ for rCPR (N = 3), $23.9 \pm 5.1 \text{ min}^{-1}$ for 147CC514 (N = 6), and $112 \pm 23.6 \text{ min}^{-1}$ for DTT-treated 147CC514 (N = 4) (Figure 3, Table 1) from the slope fitted by the least-square method. The rate of reduction in the presence of 147CC514 and DTT-treated 147CC514 was 5.1-fold and 1.1-fold slower, respectively, than that in the presence of rCPR. The data indicated that the decrease of the reduction rate was recovered by the cleavage of the disulfide bond between Cys147 and Cys514 in 147CC514. This is consistent with the results of the HO assay stated above and the rate of cytochrome *c* reduction in the presence of membrane-bound 147CC514 [27]. Previously, we reported that the rate of heme-rHO-1 reduction in the presence of ΔTGEE was 360-fold slower than that in presence of rCPR [24]. Therefore, 147CC514 was shown to be capable of reducing the ferric heme iron in heme-rHO-1 and, although its efficacy was observed to be limited, it was better than ΔTGEE .

3.3. Complex Formation between CPRs and Heme-rHO-1 Evaluated by Ultracentrifugation

Sedimentation equilibrium experiments were performed to determine the affinity in the heterodimer formation between CPRs and heme-rHO-1. The sedimentation behaviors of heme-rHO-1 complexed with ΔTGEE or 147CC514 are compared in Figure 4. According to the data obtained for 5 μM heme-rHO-1 plus 5 μM ΔTGEE , a complex model fitted well with the data with small, symmetrically distributed residuals (Figure 4A, upper and bottom panels), whereas a non-complexed model fitted poorly with the data (Figure 4A, middle and bottom panels). The K_d value of ΔTGEE for heme-rHO-1

was estimated to be $0.178 \pm 0.077 \mu\text{M}$. Conversely, the data obtained from the reaction using $5 \mu\text{M}$ heme-rHO-1 plus $5 \mu\text{M}$ 147CC514 revealed a shift in the absorbance toward a smaller radial position, suggesting a shift in the equilibrium toward a significantly larger population of monomeric proteins (compare the lower panels of Figure 4A,B). When the concentration of heme-rHO-1 and 147CC514 increased to $15 \mu\text{M}$ (maximum concentration allowing the sedimentation equilibrium measurement), we recorded a K_d value of $111 \pm 5 \mu\text{M}$ (Figure S4A). Notably, the K_d value of 147CC514 for heme-rHO-1 was reduced to $65.5 \pm 17.0 \mu\text{M}$ upon the cleavage of the disulfide linkage between Cys147 and Cys514 and was comparable to that of rCPR ($62.1 \pm 1.7 \mu\text{M}$) (compare Figure S4B,C).

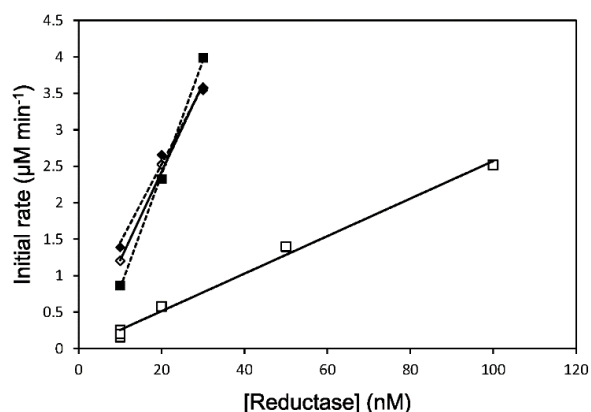


Figure 3. Rate of heme reduction in heme-rHO-1 in the NADPH-rCPR (diamonds) or NADPH-147CC514 systems (squares). The initial reduction rates of ferric heme-rHO-1 in the presence of rCPR or 147CC514 after the addition of NADPH were recorded under CO-saturated conditions. The results obtained using DTT-treated reductases are plotted as filled symbols and dashed lines. A representative example of the multiple measurements performed is displayed. See Methods for details.

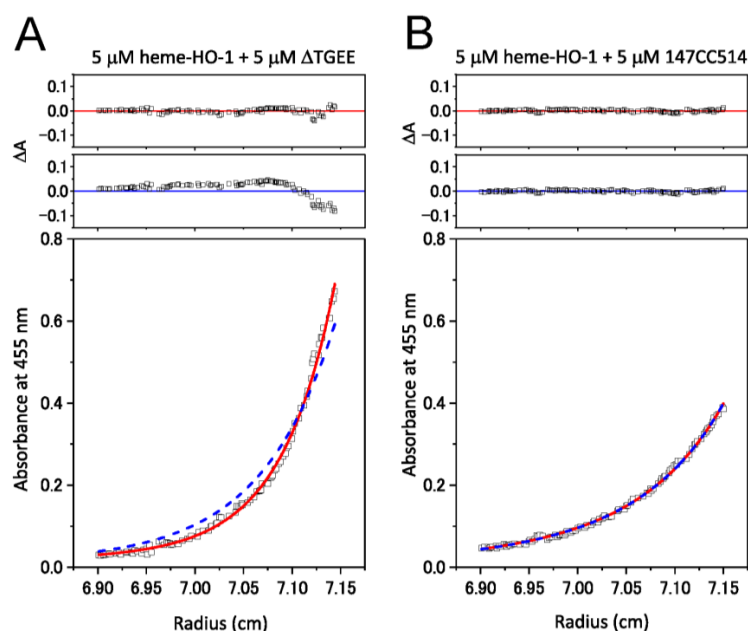


Figure 4. Sedimentation equilibrium analysis for heterodimer formation between heme-rHO-1 and ΔTGEE (A) or 147CC514 (B). The concentration of each protein was $5 \mu\text{M}$. Absorbance data were collected at 15,000 rpm in a Beckman XL-A analytical ultracentrifuge. The data points fit to the complex (red lines) and non-complexed (blue dashed lines) models. The K_d value of ΔTGEE for heme-rHO-1 was estimated to be $0.178 \pm 0.077 \mu\text{M}$. Residual fitting is depicted above both curve fits, with the complex model indicated in red, and the non-complexed model in blue.

3.4. Cryo-EM Structure of the rCPR–Heme–rHO-1 Complex

We could successfully observe single particles of the rCPR–heme–rHO-1 complex using cryo-EM. Figure 5 compares a cryo-electron microscopic image and the X-ray structure of the Δ TGEE–heme–HO-1 complex (PDB ID: 3WKT) [24]. The surface structure of rCPR–heme–rHO-1 (illustrated as a gray net in Figure 5) was consistent with the X-ray structure of the Δ TGEE–heme–HO-1 complex (ribbon diagrams in Figure 5), which confirmed that the X-ray structure represents the complex structure of rCPR–heme–HO-1 in aqueous solution.

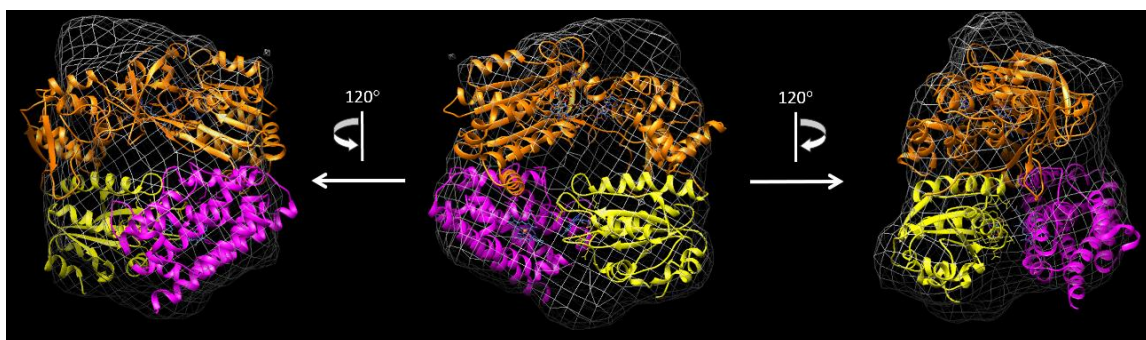


Figure 5. Three-dimensional reconstruction of the rCPR–heme–rHO-1 complex structure from a cryo-electron microscopic image (gray net); comparison with the X-ray structure of the Δ TGEE–heme–HO-1 complex (PDB ID: 3WKT). Resolution of the structure from cryo-EM was calculated as 25 Å. The X-ray crystal structures of the Δ TGEE–heme–HO-1 complex are indicated by ribbon diagrams: magenta, rHO-1; yellow, FMN domain of Δ TGEE; orange, FAD domain of Δ TGEE.

4. Discussion

Several biophysical studies on CPR, including small-angle X-ray scattering, ion-mobility separation–mass spectroscopy, NMR, and fluorescence resonance energy transfer (FRET) studies, among others, suggest the presence of a redox-linked equilibrium between the open and the closed conformations of CPR [41–44]. The recently discovered crystal structure of the complex formed between Δ TGEE and heme–rHO-1 revealed that the open form of CPR binds tightly to heme–rHO-1 and the heme residue is positioned close enough to FMN for electron transfer to occur from FMN to heme [24]. The cryo-EM map of the rCPR and heme–rHO-1 complex presented in this paper is consistent with the crystal structure, although the resolution of the EM map was lower (Figure 5). Further, we characterized HO activity, reduction kinetics, and affinity between the CPR variants and heme–rHO-1. We observed that, although heme–rHO-1 bound tightly to Δ TGEE ($K_d = 0.178 \pm 0.077 \mu\text{M}$), the reduction kinetics in the presence of Δ TGEE were considerably slow [24]. The apparent affinity of heme–rHO-1 for 147CC514 ($K_d = 111 \pm 5 \mu\text{M}$) was weaker than that for rCPR ($K_d = 62.1 \pm 1.7 \mu\text{M}$). This is consistent with the results of HO activity and reduction kinetics. The HO activity and reduction kinetics in the presence of 147CC514 were 9-fold and 5-fold lower and slower, respectively, than those in the presence of rCPR (Table 1). The sedimentation equilibrium experiment suggested that the affinity between 147CC514 and heme–rHO-1 was restored upon cleavage of the unique disulfide linkage in 147CC514, and its K_d value ($K_d = 65.5 \pm 17.0 \mu\text{M}$) was comparable to the apparent affinity between rCPR and heme–rHO-1 (Figure S4). The reduction of the disulfide bond in 147CC514 restored HO activity, reduction kinetics, and affinity of heme–rHO-1, which suggests that fixing the closed form by targeting the disulfide bond affects these characteristics.

However, 147CC514 retained the electron transfer activity to heme–rHO-1, although it was 10–20% of that of rCPR. The residual activity was consistent with the redox activity of 147CC514 with cytochrome *c* and cytochrome P450 [27]. We reasoned that a relatively small fraction of 147CC514 without the disulfide bond transfers electrons to heme–rHO-1. We crystallized 147CC514 and confirmed the formation of the disulfide bond. We observed that Cys514 has two alternative conformations: a

major conformation (refined occupancy of 0.73) in which a disulfide bond is formed with Cys147, and a minor conformation (refined occupancy of 0.27) similar to that formed after DTT treatment (Figure S1) [27]. Because X-ray reduction during data collection might have cleaved the disulfide bond although the X-ray dose was limited to 0.4 MGy, this is consistent with the residual activity of 147CC514. Therefore, we believe that the closed form of CPR does not bind heme–HO-1; however, the closed form of CPR is necessary for intramolecular electron transfer. Our data suggest that both the closed and the open forms are necessary for efficient electron transfer from CPR to heme–HO-1.

Recent NMR and FRET studies suggest that the “open–close” transition in CPR has a time scale ranging from milliseconds to seconds [41,42], whereas that of the electron transfer may range from femtoseconds to nanoseconds [45,46]. Therefore, at least 10 milliseconds to 10 seconds are required to complete an HO reaction, which requires seven transition cycles. α -Verdoheme, one of the oxygen-labile intermediates of the HO reaction, would be protected by binding to CO, which is concomitantly released with α -verdoheme. The binding of CO to α -verdoheme is also related to the redox potential of α -verdoheme [47]. α -Hydroxyheme is more oxygen-labile than α -verdoheme, and it is considerably difficult to detect the intermediate by spectroscopy. Perhaps, there is a yet undiscovered mechanism that protects α -hydroxyheme in HO or accelerates electron transfer to α -hydroxyheme in HO.

5. Conclusions

We analyzed the interaction between heme–rHO-1 and an rCPR mutant fixed in a closed conformation, 147CC514, by analytical ultracentrifugation. Further, we assayed HO activity and heme reduction activity in the presence of the NADPH–147CC514 system. The results indicate that the interaction between heme–rHO-1 and 147CC514 is considerably weak relative to that between heme–rHO-1 and the rCPR mutant fixed in an open conformation, i.e., Δ TGEE. The enzymatic activity of 147CC514 is markedly weaker than that of rCPR. In addition, we confirmed that the crystal structure of Δ TGEE in complex with heme–rHO-1 is similar to the relatively low-resolution cryo-EM structure of rCPR complexed with heme–rHO-1 in solution. Thus, CPR in the open form could be tightly bound to heme–rHO-1 for intermolecular electron transfer, and CPR in the closed form is suitable for intramolecular electron transfer between coenzymes bound to CPR. We conclude that the “open–close” transition of CPR is indispensable for a rapid “association–dissociation” cycle and a smooth electron transfer from CPR to heme–HO-1.

Supplementary Materials: The following are available online at <http://www.mdpi.com/2076-3921/9/8/673/s1>, Figure S1: (A) Close-up view of the disulfide bond in 147CC514 and (B) Comparison of our refined model with 3OJW. Figure S2: Raw timecourse data for the measurements of HO activity (A) and reduction rate (B). Figure S3: Cryo-EM data of rCPR–heme–rHO-1 complex. Figure S4: Sedimentation equilibrium analysis for heterodimer formation of heme–rHO-1 with 147CC514 (A), IAM/DTT-treated 147CC514 (B), and rCPR (C). Table S1: Crystallographic data collection and refinement statistics of 147CC514.

Author Contributions: Conceptualization, M.S., J.T., T.Y., and H.S. (Hiroshi Sakamoto); methodology, M.S., J.T., H.S. (Hideaki Sato), T.Y., and H.S. (Hiroshi Sakamoto); validation, M.S., J.T., T.S., T.Y., and H.S. (Hiroshi Sakamoto); formal analysis, M.S., J.T., T.S., R.N., T.Y., and H.S. (Hiroshi Sakamoto); investigation, M.S., J.T., T.S., R.N., T.Y., and H.S. (Hiroshi Sakamoto); resources, M.S., J.T., M.N., K.Y., T.Y., and H.S. (Hiroshi Sakamoto); writing—original draft preparation, M.S., J.T., T.Y., and H.S. (Hiroshi Sakamoto); writing—review and editing, M.S., J.T., H.S. (Hideaki Sato), M.N., K.F., K.Y., T.Y., and H.S. (Hiroshi Sakamoto); visualization, M.S., J.T., and T.Y.; supervision, M.N., K.F., K.Y., T.Y., and H.S. (Hiroshi Sakamoto); project administration, M.S., J.T., T.Y., and H.S. (Hiroshi Sakamoto); funding acquisition, M.S., J.T., M.N., and H.S. (Hiroshi Sakamoto). All authors have read and agreed to the published version of the manuscript.

Funding: This work was partly supported by JSPS KAKENHI Grant numbers 25840026, 16K07280, 19K06515 (M.S.), 16K21226 (J.T.), 24590366 (M.N.), 18K05358 (H.S. (Hiroshi Sakamoto)), by a grant from Protein Research Foundation to M.S., and by grants from Takeda Science Foundation to M.S. and J.T.

Acknowledgments: Diffraction data of 147CC514 were collected at the BL38B1 and BL44XU, SPring-8 (Proposal Nos. 2014A1040 and 2014B6963). For data collection, we thank Seiki Baba of JASRI, Kei Wada of the University of Miyazaki, and Akifumi Higashiura (present affiliation; Hiroshima University), Eiki Yamashita, and Atsushi Nakagawa of Osaka University.

Conflicts of Interest: The authors declare no conflicts of interest.

References

1. Kikuchi, G.; Yoshida, T.; Noguchi, M. Heme oxygenase and heme degradation. *Biochem. Biophys. Res. Commun.* **2005**, *338*, 558–567. [[CrossRef](#)] [[PubMed](#)]
2. Ortiz de Montellano, P.R.; Wilks, A. Heme oxygenase structure and mechanism. In *Advances in Inorganic Chemistry*; Sykes, A.G., Ed.; Academic Press: San Diego, CA, USA, 2001; Volume 51, pp. 359–407.
3. Tenhunen, R.; Marver, H.S.; Schmid, R. The enzymatic conversion of heme to bilirubin by microsomal heme oxygenase. *Proc. Natl. Acad. Sci. USA* **1968**, *61*, 748–755. [[CrossRef](#)] [[PubMed](#)]
4. Ryter, S.W.; Alam, J.; Choi, A.M. Heme oxygenase-1/carbon monoxide: From basic science to therapeutic applications. *Physiol. Rev.* **2006**, *86*, 583–650. [[CrossRef](#)] [[PubMed](#)]
5. Morikawa, T.; Kajimura, M.; Nakamura, T.; Hishiki, T.; Nakanishi, T.; Yukutake, Y.; Nagahata, Y.; Ishikawa, M.; Hattori, K.; Takenouchi, T.; et al. Hypoxic regulation of the cerebral microcirculation is mediated by a carbon monoxide-sensitive hydrogen sulfide pathway. *Proc. Natl. Acad. Sci. USA* **2012**, *109*, 1293–1298. [[CrossRef](#)] [[PubMed](#)]
6. Sugishima, M.; Wada, K.; Unno, M.; Fukuyama, K. Bilin-metabolizing enzymes: Site-specific reductions catalyzed by two different type of enzymes. *Curr. Opin. Struct. Biol.* **2019**, *59*, 73–80. [[CrossRef](#)]
7. Noguchi, M.; Yoshida, T.; Kikuchi, G. Purification and properties of biliverdin reductases from pig spleen and rat liver. *J. Biochem. (Tokyo)* **1979**, *86*, 833–848. [[CrossRef](#)]
8. Kutty, R.K.; Maines, M.D. Purification and characterization of biliverdin reductase from rat liver. *J. Biol. Chem.* **1981**, *256*, 3956–3962.
9. Schuller, D.J.; Wilks, A.; de Ortiz Montellano, P.R.; Poulos, T.L. Crystal structure of human heme oxygenase-1. *Nat. Struct. Biol.* **1999**, *6*, 860–867.
10. Sugishima, M.; Omata, Y.; Kakuta, Y.; Sakamoto, H.; Noguchi, M.; Fukuyama, K. Crystal structure of rat heme oxygenase-1 in complex with heme. *FEBS Lett.* **2000**, *471*, 61–66. [[CrossRef](#)]
11. Sugishima, M.; Sakamoto, H.; Kakuta, Y.; Omata, Y.; Hayashi, S.; Noguchi, M.; Fukuyama, K. Crystal structure of rat apo-heme oxygenase-1 (HO-1): Mechanism of heme binding in HO-1 inferred from structural comparison of the apo and heme complex forms. *Biochemistry* **2002**, *41*, 7293–7300. [[CrossRef](#)]
12. Sugishima, M.; Sakamoto, H.; Higashimoto, Y.; Noguchi, M.; Fukuyama, K. Crystal structure of rat heme oxygenase-1 in complex with biliverdin-iron chelate: Conformational change of the distal helix during the heme cleavage reaction. *J. Biol. Chem.* **2003**, *278*, 32352–32358. [[CrossRef](#)] [[PubMed](#)]
13. Sugishima, M.; Sakamoto, H.; Noguchi, M.; Fukuyama, K. Crystal structures of ferrous and CO-, CN⁻, and NO-bound forms of rat heme oxygenase-1 (HO-1) in complex with heme: Structural implications for discrimination between CO and O₂ in HO-1. *Biochemistry* **2003**, *42*, 9898–9905. [[PubMed](#)]
14. Sato, H.; Sugishima, M.; Sakamoto, H.; Higashimoto, Y.; Shimokawa, C.; Fukuyama, K.; Palmer, G.; Noguchi, M. Crystal structure of rat haem oxygenase-1 in complex with ferrous verdohaem: Presence of a hydrogen-bond network on the distal side. *Biochem. J.* **2009**, *419*, 339–345. [[CrossRef](#)] [[PubMed](#)]
15. Sugishima, M.; Moffat, K.; Noguchi, M. Discrimination between CO and O₂ in heme oxygenase: Comparison of static structures and dynamic conformation changes following CO photolysis. *Biochemistry* **2012**, *51*, 8554–8562. [[PubMed](#)]
16. Unno, M.; Matsui, T.; Chu, G.C.; Couture, M.; Yoshida, T.; Rousseau, D.L.; Olson, J.S.; Ikeda-Saito, M. Crystal structure of the dioxygen-bound heme oxygenase from *Corynebacterium diphtheriae*: Implications for heme oxygenase function. *J. Biol. Chem.* **2004**, *279*, 21055–21061. [[CrossRef](#)] [[PubMed](#)]
17. Unno, M.; Matsui, T.; Ikeda-Saito, M. Structure and catalytic mechanism of heme oxygenase. *Nat. Prod. Rep.* **2007**, *24*, 553–570. [[CrossRef](#)] [[PubMed](#)]
18. Unno, M.; Matsui, T.; Ikeda-Saito, M. Crystallographic studies of heme oxygenase complexed with an unstable reaction intermediate, verdoheme. *J. Inorg. Biochem.* **2012**, *113*, 102–109. [[CrossRef](#)]
19. Unno, M.; Ardevol, A.; Rovira, C.; Ikeda-Saito, M. Structures of the substrate-free and product-bound forms of HmuO, a heme oxygenase from corynebacterium diphtheriae: X-ray crystallography and molecular dynamics investigation. *J. Biol. Chem.* **2013**, *288*, 34443–34458. [[CrossRef](#)]
20. Pandey, A.V.; Fluck, C.E. NADPH P450 oxidoreductase: Structure, function, and pathology of diseases. *Pharmacol. Ther.* **2013**, *138*, 229–254. [[CrossRef](#)]
21. Iyanagi, T.; Xia, C.; Kim, J.J. NADPH-cytochrome P450 oxidoreductase: Prototypic member of the diflavin reductase family. *Arch. Biochem. Biophys.* **2012**, *528*, 72–89. [[CrossRef](#)]

22. Wang, M.; Roberts, D.L.; Paschke, R.; Shea, T.M.; Masters, B.S.; Kim, J.J. Three-dimensional structure of NADPH-cytochrome P450 reductase: Prototype for FMN- and FAD-containing enzymes. *Proc. Natl. Acad. Sci. USA* **1997**, *94*, 8411–8416. [[CrossRef](#)] [[PubMed](#)]
23. Hamdane, D.; Xia, C.; Im, S.C.; Zhang, H.; Kim, J.J.; Waskell, L. Structure and function of an NADPH-cytochrome P450 oxidoreductase in an open conformation capable of reducing cytochrome P450. *J. Biol. Chem.* **2009**, *284*, 11374–11384. [[CrossRef](#)] [[PubMed](#)]
24. Sugishima, M.; Sato, H.; Higashimoto, Y.; Harada, J.; Wada, K.; Fukuyama, K.; Noguchi, M. Structural basis for the electron transfer from an open form of NADPH-cytochrome P450 oxidoreductase to heme oxygenase. *Proc. Natl. Acad. Sci. USA* **2014**, *111*, 2524–2529. [[CrossRef](#)] [[PubMed](#)]
25. Sugishima, M.; Sato, H.; Wada, K.; Yamamoto, K. Crystal structure of a NADPH-cytochrome P450 oxidoreductase (CYPOR) and heme oxygenase 1 fusion protein implies a conformational change in CYPOR upon NADPH/NADP(+) binding. *FEBS Lett.* **2019**, *593*, 868–875. [[CrossRef](#)]
26. Spencer, A.L.; Bagai, I.; Becker, D.F.; Zuiderweg, E.R.; Ragsdale, S.W. Protein/protein interactions in the mammalian heme degradation pathway: Heme oxygenase-2, cytochrome P450 reductase, and biliverdin reductase. *J. Biol. Chem.* **2014**, *289*, 29836–29858. [[CrossRef](#)]
27. Xia, C.; Hamdane, D.; Shen, A.L.; Choi, V.; Kasper, C.B.; Pearl, N.M.; Zhang, H.; Im, S.C.; Waskell, L.; Kim, J.J. Conformational changes of NADPH-cytochrome P450 oxidoreductase are essential for catalysis and cofactor binding. *J. Biol. Chem.* **2011**, *286*, 16246–16260. [[CrossRef](#)]
28. Iijima, M.; Ohnuki, J.; Sato, T.; Sugishima, M.; Takano, M. Coupling of Redox and Structural States in Cytochrome P450 Reductase Studied by Molecular Dynamics Simulation. *Sci. Rep.* **2019**, *9*, 9341. [[CrossRef](#)]
29. Sugishima, M.; Sakamoto, H.; Higashimoto, Y.; Omata, Y.; Hayashi, S.; Noguchi, M.; Fukuyama, K. Crystal structure of rat heme oxygenase-1 in complex with heme bound to azide. Implication for regiospecific hydroxylation of heme at the alpha-meso carbon. *J. Biol. Chem.* **2002**, *277*, 45086–45090. [[CrossRef](#)]
30. Hayashi, S.; Omata, Y.; Sakamoto, H.; Hara, T.; Noguchi, M. Purification and characterization of a soluble form of rat liver NADPH-cytochrome P-450 reductase highly expressed in Escherichia coli. *Protein Expr. Purif.* **2003**, *29*, 1–7. [[CrossRef](#)]
31. Kabsch, W. XDS. *Acta Crystallogr. Sect. D Biol. Crystallogr.* **2010**, *66*, 125–132. [[CrossRef](#)]
32. Murshudov, G.N.; Skubak, P.; Lebedev, A.A.; Pannu, N.S.; Steiner, R.A.; Nicholls, R.A.; Winn, M.D.; Long, F.; Vagin, A.A. REFMAC5 for the refinement of macromolecular crystal structures. *Acta Crystallogr. Sect. D Biol. Crystallogr.* **2011**, *67*, 355–367. [[CrossRef](#)]
33. Collaborative Computational Project No.4. The CCP4 suite: Programs for protein crystallography. *Acta Crystallogr. Sect. D Biol. Crystallogr.* **1994**, *50*, 760–763. [[CrossRef](#)] [[PubMed](#)]
34. Yoshida, T.; Takahashi, S.; Kikuchi, G. Partial purification and reconstitution of the heme oxygenase system from pig spleen microsomes. *J. Biochem. (Tokyo)* **1974**, *75*, 1187–1191. [[CrossRef](#)]
35. Sun, D.; Sato, M.; Yoshida, T.; Shimizu, H.; Miyatake, H.; Adachi, S.; Shiro, Y.; Kikuchi, A. Crystallization and preliminary X-ray diffraction analysis of a rat biliverdin reductase. *Acta Crystallogr. Sect. D Biol. Crystallogr.* **2000**, *56*, 1180–1182. [[CrossRef](#)]
36. Yoshida, T.; Kikuchi, G. Purification and properties of heme oxygenase from pig spleen microsomes. *J. Biol. Chem.* **1978**, *253*, 4224–4229. [[PubMed](#)]
37. Lebowitz, J.; Lewis, M.S.; Schuck, P. Modern analytical ultracentrifugation in protein science: A tutorial review. *Protein Sci.* **2002**, *11*, 2067–2079. [[CrossRef](#)] [[PubMed](#)]
38. Yasunaga, T.; Wakabayashi, T. Evaluation of a 2k CCD camera with an epitaxially grown CsI scintillator for recording energy-filtered electron cryo-micrographs. *J. Electron Microsc. (Tokyo)* **2008**, *57*, 101–112. [[CrossRef](#)] [[PubMed](#)]
39. Yasunaga, T.; Wakabayashi, T. Extensible and object-oriented system Eos supplies a new environment for image analysis of electron micrographs of macromolecules. *J. Struct. Biol.* **1996**, *116*, 155–160. [[CrossRef](#)]
40. Murakami, K.; Yasunaga, T.; Noguchi, T.Q.; Gomibuchi, Y.; Ngo, K.X.; Uyeda, T.Q.; Wakabayashi, T. Structural basis for actin assembly, activation of ATP hydrolysis, and delayed phosphate release. *Cell* **2010**, *143*, 275–287. [[CrossRef](#)]
41. Pudney, C.R.; Khara, B.; Johannissen, L.O.; Scrutton, N.S. Coupled motions direct electrons along human microsomal P450 Chains. *PLoS Biol.* **2011**, *9*, e1001222. [[CrossRef](#)]

42. Frances, O.; Fatemi, F.; Pompon, D.; Guittet, E.; Sizun, C.; Perez, J.; Lescop, E.; Truan, G. A well-balanced preexisting equilibrium governs electron flux efficiency of a multidomain diflavin reductase. *Biophys. J.* **2015**, *108*, 1527–1536. [[CrossRef](#)] [[PubMed](#)]
43. Jenner, M.; Ellis, J.; Huang, W.C.; Lloyd Raven, E.; Roberts, G.C.; Oldham, N.J. Detection of a protein conformational equilibrium by electrospray ionisation-ion mobility-mass spectrometry. *Angew. Chem. Int. Ed. Engl.* **2011**, *50*, 8291–8294. [[CrossRef](#)]
44. Huang, W.C.; Ellis, J.; Moody, P.C.; Raven, E.L.; Roberts, G.C. Redox-linked domain movements in the catalytic cycle of cytochrome p450 reductase. *Structure* **2013**, *21*, 1581–1589. [[CrossRef](#)] [[PubMed](#)]
45. Moser, C.C.; Keske, J.M.; Warncke, K.; Farid, R.S.; Dutton, P.L. Nature of biological electron transfer. *Nature* **1992**, *355*, 796–802. [[CrossRef](#)] [[PubMed](#)]
46. Henzler-Wildman, K.A.; Lei, M.; Thai, V.; Kerns, S.J.; Karplus, M.; Kern, D. A hierarchy of timescales in protein dynamics is linked to enzyme catalysis. *Nature* **2007**, *450*, 913–916. [[CrossRef](#)] [[PubMed](#)]
47. Sato, H.; Higashimoto, Y.; Sakamoto, H.; Sugishima, M.; Shimokawa, C.; Harada, J.; Palmer, G.; Noguchi, M. Reduction of oxaporphyrin ring of CO-bound alpha-verdoheme complexed with heme oxygenase-1 by NADPH-cytochrome P450 reductase. *J. Inorg. Biochem.* **2011**, *105*, 289–296. [[CrossRef](#)] [[PubMed](#)]



© 2020 by the authors. Licensee MDPI, Basel, Switzerland. This article is an open access article distributed under the terms and conditions of the Creative Commons Attribution (CC BY) license (<http://creativecommons.org/licenses/by/4.0/>).